RESEARCH ARTICLE

Influence of preparation techniques of cellulose II nanocrystals as reinforcement for tannery solid waste–based gelatin composite films

Vimudha Muralidharan[1,2] · Saiprasad Gochhayat[3] · Saravanan Palanivel[2,4] · Balaraman Madhan[1,2]

Abstract

Tannery waste–based gelatin composite film reinforced with cellulose II nanocrystal (CNC II) extracted from wet wipes using three different hydrolysis techniques is explored for its functional properties and possible utilization as a biodegradable packaging material. CNC II isolated using hydrogen peroxide (PCNC), citric acid (CCNC), and hydrochloric acid (HCNC) differed in morphological and crystalline character as investigated using DLS, FE-SEM, FTIR, and XRD analysis. The crystallinity of PCNC, CCNC, and HCNC was found to be 81.1%, 75.4%, and 86.1%, respectively. The highly crystalline CNC II (PCNC) incorporation improved mechanical stiffness of rawhide trimming waste–based gelatin films by 50% compared to control gelatin film. Maximum thermal decomposition with T_{max} of 329 °C was obtained for gelatin films with PCNC nano-reinforcement. Films with CNC II were structurally stable and sufficiently antibacterial against Gram-positive *S. aureus* microbial strain. Strong interfacial non-covalent and hydrogen bonding interactions between gelatin and cellulose II nanocrystal have likely enhanced the properties of the composite films. Incorporation of CNC II reduced the surface wettability of the films and nanocomposites absorbed UV radiation as evidenced by transmittance value T_{280} of 0.19%. Nanocomposite films degraded up to 79.9% of initial mass within 7 days of soil burial. Furthermore, based on the optimized system, single-use packaging application of eggplant seeds has been demonstrated.

Keywords Cellulose II nanocrystal · Wet wipes · Leather waste · Gelatin · Biodegradable packaging

✉ Balaraman Madhan
  bmadhanscience@gmail.com; madhan@clri.res.in

1   Centre for Academic and Research Excellence (CARE), CSIR-Central Leather Research Institute, Adyar, Chennai, Tamil Nadu 600 020, India

2   Department of Leather Technology, A C Tech (Housed at CSIR-CLRI), Anna University, Chennai, Tamil Nadu 600 025, India

3   Department of Chemical Engineering, BITS-Pilani, Hyderabad Campus, Hyderabad, Telangana 500 078, India

4   Leather Process Technology Department, CSIR-Central Leather Research Institute, Adyar, Chennai, Tamil Nadu 600 020, India

Introduction

Plastics are ubiquitous in every aspect of life. The plastic material is so prevalent in the recent times that the twentieth and twenty-first centuries have justifiably been called the "Plastic age." The production and consumption of plastics, especially single-use packaging plastics, have increased steadily over time. As a result, the accumulation of plastic as solid wastes in the environment is dangerously alarming. By 2050, it is expected that roughly around 12 billion tons of plastic waste will end up in landfills or natural environment (Geyer et al. 2017). The plastic substrates photodegrade into micro-size (<5 mm in size) under long exposure to UV radiation. These particulate matters pervade the environment and reach every stratum of the atmosphere. Primary sources of microplastics in the environment include microbeads generated from cosmetic products, large plastic wastes, microfiber from non-woven textile, and sanitary product waste including wet wipes (Briain et al. 2020).

Research on biodegradable materials based on biopolymers or from renewable sources have been sought after as one of the plastic pollution abatement strategies, besides plastic recycling. Biopolymers, both protein and polysaccharide-based ones are the popular kind of plastic alternatives. Utilizing industrial wastes as renewable feedstock for preparing biodegradable plastic would solve plastic pollution as well as waste accumulation issue.

Tanning industry utilizes rawhides and skins as raw material with copious amount of water and chemical inputs, in order to manufacture leather. As much as 35 m^3 of wastewater and 800 kg of solid wastes are generated during the leather production from 1 ton of rawhides and skins (Kandasamy et al. 2020). Among the solid wastes, trimming wastes are the unwanted offal pieces trimmed and disposed of, contributing to the major proportion. According to FAO report, around 418 thousand tons of raw trimming wastes is generated per year (FAO 2013). Trimming wastes are rich in protein in the form of collagen and hair keratin. These wastes have been exhaustively utilized for preparation of several low-value and high-value components applicable for leather manufacturing, polymeric applications, adhesive and textile application (Sathish et al. 2019; Andonegi et al. 2020; Liu et al. 2011). The gelatin extracted from the trimming wastes would be a suitable biodegradable alternative owing to its multifunctional polyelectrolyte nature and film forming ability. Earlier, our research group has attempted the preparation of gelatin films with PVA, targeting to enhance its characteristics for packaging applications (Masilamani et al. 2017).

One of the most popular strength enhancement strategies include reinforcement of the gelatin matrix with functional nano-fillers. Cellulose nanocrystals (CNCs) are polysaccharide-based nanomaterials that are used in many applications including food packaging and preservation (Noorbakhsh-Soltani et al. 2018; Xiao et al. 2021). CNCs can be extracted from several plant sources (Beltramino et al. 2015; Moran et al. 2008; Xu et al. 2013), animal sources such as from tunicate (Zhao et al. 2015), agricultural wastes (De et al. 2021), and bacterial cellulosic sources (George and Siddaramaiah 2012). As a nanomaterial, CNCs exhibit an array of properties such as high crystallinity, large surface area, biodegradability, and large aspect ratio with surface functionalities. Nanocomposites prepared using protein and CNC have been used for sustained curcumin delivery (Wang et al. 2020) or as heavy metal adsorption hydrogel beads in combination with carboxylated chitosan or sodium alginate matrix (Xu et al. 2021; Zhao et al. 2021). Cellulose is a linear homopolysaccharide composed of both crystalline and amorphous regions. The molecular orientation and functionalities in crystalline region vary widely giving rise to four major polymorphs of cellulose, viz., cellulose I, cellulose II, cellulose III, and cellulose IV. Majority of the native cellulose exists in the type I polymorph and can be converted to other polymorph type by chemical transformations.

Wet wipes are viscose textile-based materials that are marketed as biodegradable and ecofriendly. But these products form a significant component of global sewerage system blockages (Briain et al. 2020). Wet wipes have been part of everyday hygiene, gaining more attention ever so more since the COVID-19 pandemic. The viscose material is the mercerized form of cellulose that forms the raw material for wet wipe manufacturing. Mercerization of cellulose using concentrated sodium hydroxide solution or dissolution/regeneration using a cellulose solvent such as N-methylmorpholine N-oxide (NMMO) or ionic liquids converts the cellulose polymorph I to cellulose II polymorph (Jin et al. 2016). Recently, a caustic-free system consisting of mildly acidic lithium bromide trihydrate (MALBTH) solution (a green solvent) achieved selective hydrolysis of disordered cellulose and cellulose polymorph conversion simultaneously (Li et al. 2021). In contrast to cellulose I, cellulose II has more stable structure making it suitable for several applications (Mansikkamaki et al. 2007). Cellulose II nanocrystals that have been extracted from mercerized cellulose I are renewable, biodegradable, and non-toxic materials used in biomaterials due to their enhanced mechanical properties, low density, and low thermal expansion (Du et al. 2019). Extraction of CNCs for biomaterial reinforcement conventionally uses strong mineral acids such as sulfuric acid that leads to over degradation of cellulose, large quantities of water, and large amount of salt disposal as waste that are difficult to recover and reuse (Chen et al. 2016). Alternative to strong sulfuric acid, using mineral acid (hydrochloric acid) and organic acids has been reported so far (Jiang et al. 2010).

In the present work, for the first time, we report the extraction of cellulose II nanocrystal (CNC II) from wet wipe cellulose using three different hydrolysis techniques and characterized for its reinforcement efficiency on physical and chemical properties of trimming waste–based gelatin nanocomposite films. The nanocomposite films were also characterized for their biopolymeric functionalities to replace conventional plastic substrates as single-use packaging material.

Materials and methods

Materials

Delimed dehaired bovine trimming wastes were collected from Leather Processing Technology Department (LPTD), CSIR-CLRI, India. Wet tissue wipes were procured from the brand Kara wet wipes. Analytical grade sodium hydroxide pellets and sodium silicate were procured from M/s S-D Fine Chem Ltd., and sodium dodecyl sulfate (SDS) was obtained

from M/s HiMedia. Dihydrogen peroxide (99.5% purity) was obtained from M/s Merck. Acetic acid and citric acid were obtained from SRL Chemicals (Chennai, India). Nutrient broth and Mueller Hinton HiVeg agar for antimicrobial tests were procured from M/s HiMedia Pvt. Ltd. Soil (20% moisture) was procured from a local garden in Chennai, India.

Methods

Preparation of high bloom strength gelatin from trimming wastes

High bloom strength gelatin was extracted from the pretreated bovine trimmings according to the method described by Masilamani et al. (2017), with slight modifications. Briefly, the extraction of gelatin was carried out using 0.5 M acetic acid at a temperature of 70 °C for 7 h under thermoregulated water bath setup. Gelatin in solubilized form was filtered using double mesh cloth and collected in a polystyrene tray, kept for drying at room temperature for 16 h. The dried gelatin film was peeled off the tray and pulverized to form gelatin powder.

Pretreatment of wet wipes

Wet wipes were taken from the pack and dried at 60 °C for 12 h to remove all moist components including fragrance from the wipes. The dried weight was noted, and a known number of dried wipes were manually shredded into pieces of size 2 × 2 cm. A known amount of dried shredded pieces was added to the pretreatment solution that comprised of 250 mL solution of 2% w/v NaOH, 5% w/v sodium silicate, and 0.06% w/v SDS maintained at 80 °C with constant stirring for 4 h. The obtained pulp was quenched with 750 mL cold water, washed and filtered with deionized water several times using Buchner funnel until neutrality of pH. The pulp mass was then transferred to pre-weighed crucible and dried at 60 °C for 16–17 h. The yield of cellulosic pulp was calculated based on the weight difference calculation before and after the process.

Extraction of cellulose nanocrystals by hydrolysis methods

Alkaline peroxide method

Under this method, the hydrogen peroxide 3% w/v was added dropwise to the dried shredded wet wipes submerged in the pretreatment solution and stirred vigorously at 80 °C for 4 h. The resultant turbid solution with cellulose nanocrystal (CNC, labelled as PCNC) was quenched with cold water and filtered as described in previous section.

Acidic hydrolysis method

The pretreated cellulose pulp was taken as starting material for acid-catalyzed hydrolysis method. Hydrolysis using citric acid catalyst was carried out using slightly modified method from Nagarajan et al. (2020). Briefly, citric acid solution (76% w/v) was prepared and heated at 80 °C for 30 min. After the homogeneous solution was prepared, 2 g of pretreated pulp was added to the hot citric acid solution and stirred for 4 h. The reaction was quenched by adding 250 mL of cold deionized water (10 ± 2 °C) and then washed and filtered several times until the pH was neutral. The nanocellulosic suspension (labelled as CCNC) was then dried at 60 °C for 17 h.

Another set of acid-catalyzed hydrolysis of pretreated cellulose pulp was carried out using 3M HCl solution at 1:30 w/v cellulose to solution ratio. The pulp was added to the acid solution and left to be static for 15 min. The mixture was stirred for 45 min at 450 rpm at 80 °C. The CNC II (labelled as HCNC) was then separated in dry state as described above.

Yield of the extracted cellulose nanocrystals was calculated by weight ratio between dried nanocellulose and initial weight of pretreated cellulosic pulp taken for hydrolysis reaction.

Characterization of CNCs

Particle size analysis

The particle size distribution of cellulose nanocrystals was determined by dynamic light scattering (DLS) using Zetasizer Nano ZS (Malvern Instruments Ltd.,). Nanocrystals were first dispersed in water to give 0.04 wt% solution for size determination.

Morphological assessment and light transmittance of CNC II

The surface morphological assessment of the cellulose nanocrystal was analyzed using field emission-scanning electron microscope (FE-SEM, TESCAN CLARA, Czech Republic) operated at 80-kV acceleration voltage. CNC suspension of 0.01 wt% was prepared with Millipore water, and the aqueous suspension was sonicated for 5 min. A drop of sonicated suspension was deposited onto the stub and sputter coated with 5-nm colloidal gold for dimensional analysis. Light transmittance of 0.1 wt% CNC suspension was observed using UV-Vis spectrophotometer (JASCO V760) at 600 nm.

X-ray crystallography of nanocellulose

The crystallinity index was determined by X-ray diffraction (XRD) by MiniFlex II Desktop X-ray Diffractometer (Rigaku, Japan). The samples were exposed to the X-ray beam irradiated at voltage of 30 kV and 15-mA current. Scattered radiation was detected at ambient temperature in the angular region (2θ) of 5–80° at a rate of 5°/s and a step size of 0.02°. Segal's method (Segal et al. 1959) was used to calculate the crystallinity index (CrI) by using the following equation:

$$CrI = \frac{I(ac) - I(am)}{I(ac)} \times 100 \qquad (1)$$

where $I_{(ac)}$ is the maximum intensity of the peak (020) and $I_{(am)}$ is the lowest intensity between the planes (110) and (020).

The crystallite size was estimated from XRD patterns using Scherrer equation (Normand et al. 2014):

$$D_{hkl} = K\lambda/\beta_{1/2}\cos\theta \qquad (2)$$

where D_{hkl} is the crystallite dimension in the direction normal to the (h k l) lattice planes, K is the Scherrer constant equal to 0.9, λ is the radiation wavelength (λ=0.154 nm for Cu Kα), θ is the diffraction angle, and $\beta_{1/2}$ is the peak width at the half-maximum intensity in radians.

Spectral characterization of nanocellulose (FTIR)

The hydrolyzed cellulose from wet wipes was structurally analyzed using FTIR spectrophotometer (JASCO FT/IR 4200) by KBr method. The FTIR spectra of all samples were recorded in the wavenumber band ranging between 4000 and 400 cm^{-1} and at a resolution of 4 cm^{-1}.

Preparation of nanocomposite blend films

Nanocomposite film using trimming waste gelatin and wet wipe nanocellulose were prepared by solution casting technique. One gram of waste extracted gelatin was dissolved in 5 mL of 0.5M acetic acid solution and stirred for 45 min at 40 °C. Cellulose nanocrystal from each batch of hydrolysis was added at concentration levels of 5%, 10%, and 15% (weight based on gelatin). The nanocellulose suspension was prepared by adding the required amount of CNC to 5 mL of distilled water and stirred for 45 min at room temperature. The gelatin solution was then added to the cellulose suspension and glycerol (20% w/w of total solids) was added as plasticizer. This composite blend was stirred continuously at 40 °C for 30 min and poured on levelled petri dishes of 9-cm diameter. The nanocomposite films were labelled as GPCNC5 (5%), GPCNC10 (10%), and GPCNC15 (15%) for films prepared with different concentrations of PCNC nanoparticle and a fixed quantity of gelatin. Similarly, the other films were also labelled accordingly as GCCNC for gelatin and citric acid–hydrolyzed CNC II and GHCNC for gelatin and HCl–hydrolyzed CNC II. Nanocomposite film prepared with gelatin and glycerol but without CNC II was labelled as "Control." The dried nanocomposite films were later peeled off and conditioned at 25 °C until further characterizations.

Characterization of films

Mechanical properties of films

Thickness, tensile strength, and elongation at break values were evaluated for all the nano-biocomposite films with a universal testing machine (UTM, Instron 3369/J7257, controlled by Blue-hill software, version 3). Specimens of size 5 × 1 cm were cut from the film samples. The gauge separation was kept as 30 mm. The crosshead speed was at 25 mm/min. The tests were carried out at 25 °C temperature and 50% relative humidity. Three specimens from each sample were taken and average with standard deviation are reported.

ATR-FTIR characterization of films

All nanocomposite film samples were analyzed by FTIR spectrophotometer (JASCO FT/IR 4200) operating in the attenuated total reflectance (ATR) mode. Spectra was recorded at 4000–400 cm^{-1} region at a resolution of 4 cm^{-1} at room temperature. The empty crystal was used as a background. The angle of incidence for ATR crystal was 45°.

Thermal characterization of films

Thermogravimetric analysis (TGA) was carried out on a Q50 equipment (TA instruments, Waters Austria) using a heating rate of 10 °C/min from 25 °C to 600 °C under synthetic air atmosphere. A measured quantity of 5-mg sample was conditioned in a ventilated climatic chamber at 25 ± 2 °C and 50 ± 5% RH for 48 h.

Differential scanning calorimeter (DSC) (Q200, TA instruments, Waters, Austria) was used to determine thermal properties of bio-nanocomposite films. Sample weighing 5 ± 0.3 mg was taken from the film samples and placed in sample pan with an empty reference pan. Samples were scanned at a heating rate of 10 °C/min from 30 to 300 °C, under nitrogen atmosphere, to determine the thermal stability of films.

Transparency and optical properties of films

Transparency of the gelatin-CNC films were recorded using UV-Vis spectrophotometer (JASCO V760). Samples of size 4 cm × 0.9 cm were cut from each batch and transmittance (%T) at 600 nm was recorded in triplicates according to ASTM 2003. Transparency (T_{600}) was determined as per the following equation:

$$T = -\log\left(T_{600}\right)/x \tag{3}$$

where "x" is the film thickness (in mm).

Transmittance between 200 and 800 nm was also measured using spectrophotometer to determine UV-Vis barrier ability. Light barring capacity of the films were determined at wavelength 280 nm and 660 nm.

Moisture sensitivity of films

To determine the moisture content, 1 cm × 1 cm square sized specimens were cut from the composite films of each batch. The initial weight was noted to be W_0. The specimen was dried at 100 °C for 24 h. The weight was recorded to be W_1. The weight loss expressed in percentage relative to the initial weight is given as moisture content (Eq. 4). The dried samples were then immersed in 10 mL of distilled water and incubated at ambient temperature for 3 h. Decanting the water out, the weight of the swollen matrix was recorded as W_2, and finally, the matrix was oven-dried at 100 °C for 24 h, and the resultant weight was recorded as W_3. The following calculations were done, to determine the initial moisture content, degree of swelling, and solubility of the composite films.

$$\text{Initial Moisture content} = \frac{W_0 - W_1}{W_0} \times 100 \tag{4}$$

$$\text{Degree of Swelling} = \frac{W_2 - W_1}{W_1} \tag{5}$$

$$\text{Solubility} = \frac{W_1 - W_3}{W_1} \times 100 \tag{6}$$

Water contact angle

For determining water contact angle of composite film, films with dimension of 1 cm × 1 cm specimen were cut from each sample and attached to the platform of contact angle meter. Five microliters of distilled water was dropped onto both sides of the sample and image was captured. ImageJ software was used to measure the contact angle from the droplet images.

Antimicrobial tests of nanocomposite films

The antibacterial activity of film samples set GPCNC5, GCCNC5, and GHCNC5 (labelled as P5, C5, and H5, respectively) and GPCNC15, GCCNC15, and GHCNC15 (labelled as P15, C15, and H15, respectively) with control gelatin film (labelled as G) was determined against gram-positive *Staphylococcus aureus* and gram-negative *Escherichia coli* as model pathogenic organisms by disc diffusion method. The bacteria were sub-cultured in nutrient broth (NB) medium followed by incubation at 27–30 °C for 18–24 h. The inoculum was diluted in NB medium to match turbidity = 0.5 as that of McFarland Barium sulfate standard, and 100 µL was spread over Mueller-Hinton Agar (MHA) plates. Dried, sterile disks of ø 10 mm were placed onto the inoculated petri plates and incubated for 12 h at ambient temperature for bacterial growth. The antibacterial activity was investigated by the presence of inhibition of growth zones around the film discs.

Biodegradability of films

Biodegradation under soil burial conditions were carried out under laboratory scale following the methodology as proposed by ASTM D6400 (Luchese et al. 2021). Samples of size 2 × 2 cm were weighed and covered with a thin gauze pocket with label. These samples were buried under soil (20% moisture) in a pot at a depth of 4 cm to assure aerobic degradation. The soil was moistened with water once a day. The sample from each batch was removed from soil and dried in an oven at 50 °C for 2 h. The biodegradation rate was calculated by the weight loss percentage at the final day of observation. The digital images of the degraded samples were captured to record the biodegradation.

Packaging potential of films

A sample of prepared film (control gelatin and GPCNC15) was thermally sealed with heat sealing machine packed with seeds of eggplant. The sealed packets were maintained at room temperature to monitor the performance of the films as disposable packaging films.

Statistical analysis

Statistical analysis of the data was evaluated using GraphPad Prism 8 (GraphPad Inc., San Diego, CA, USA). All data are reported as mean and standard deviation for triplicates. One-way ANOVA (analysis of variance) was conducted to determine the statistical significance at $p < 0.05$ (95% confidence)

level. Post hoc Tukey's test was done followed by ANOVA to compare the means of different groups for identifying the significant differences at $p<0.05$ and $p<0.01$ (99% confidence) level for light transmittance experiments.

Results and discussion

Characterization of cellulose nanocrystal (CNC) from wet wipes

Yield, particle size, and zeta potential of CNC

The schematic for preparation of cellulose II nanocrystal from wet wipes is illustrated in Fig. 1. The current strategy of CNC II preparation without use of mercerization was done under least number of purification steps. The simple process of Buchner filtration with few cycles of washing for neutralization was carried out for CNC II purification. The yield, particle size, and zeta potential of pretreated pulp and CNCs are given in Table 1. The yield of pretreated pulp from dried wet wipe was determined as 72%. The pretreated pulp devoid of chemicals from the wet wipe was used as precursor for the CNC preparation. The yield from peroxide treatment was found to be 66%. This was higher than the yield of cellulose nanoparticles prepared from softwood pulp by H_2O_2 oxidation (54%) (Koshani et al. 2018). The yield of CCNC was found to be 81%. The citric acid at 76 wt% was sufficient to cleave the glycosidic bonds between the fibrils leading to depolymerization and high recovery of cellulose nanocrystal. The current work led to higher yield of CCNC compared to the previous reports (Nagarajan et al. 2020; Ji
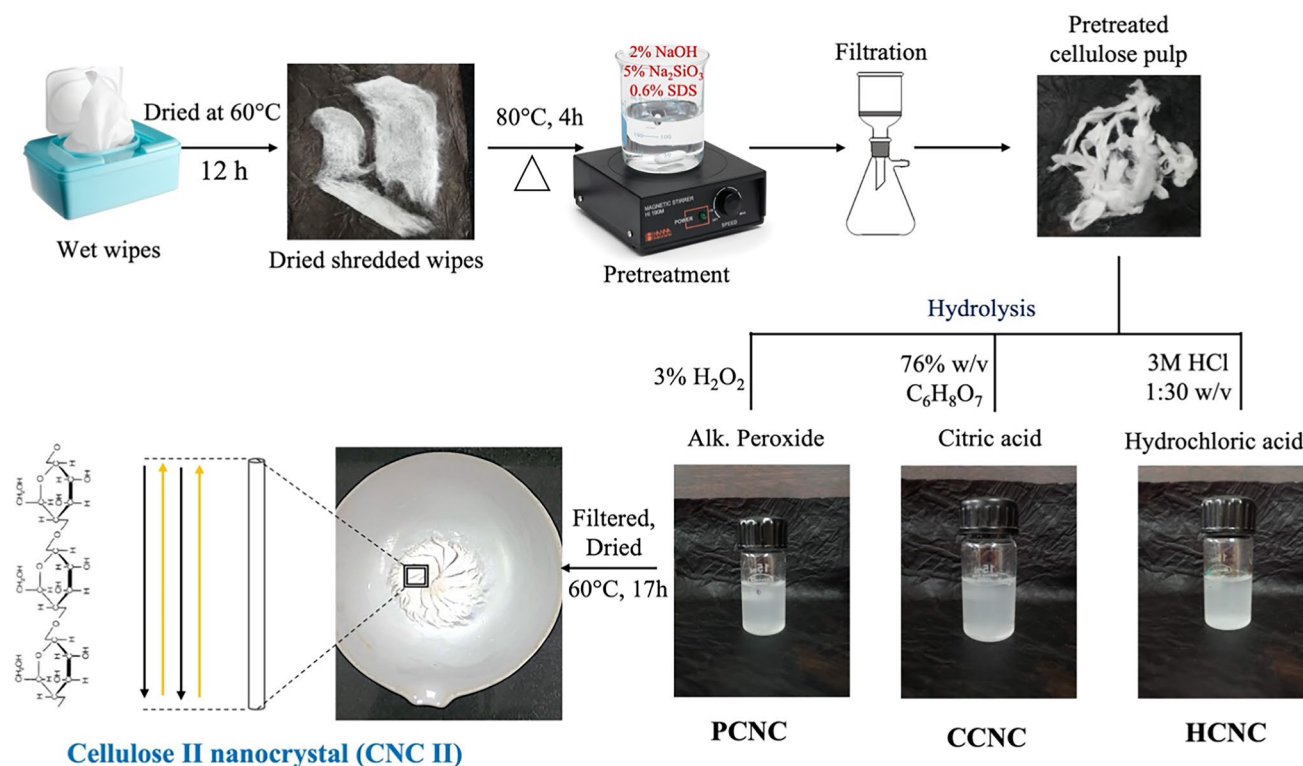
Fig. 1 Schematic illustration of cellulose II nanocrystal preparation from wet wipes

Table 1 Characteristics of CNC II nanoparticles prepared by different hydrolysis techniques

Sample	Particle size (nm)	Zeta potential (mV)	Yield (%)	CS (nm)	CrI (%)	CrR (%)
Pretreated Pulp	-	-	72	2.35	62.0	0.804
PCNC	248.7 ± 1.11	−23.0 ± 0.34	66	4.49	81.1	0.265
CCNC	141.8 ± 2.52	−19.9 ± 0.87	81	5.39	75.4	0.216
HCNC	128.7 ± 3.24	−24.9 ± 0.23	77	5.5	86.1	2.565

[*]Mean ± standard deviation ($n=3$)

et al. 2019). The hydrochloric acid–based CNC extraction method resulted in 77% yield. The mineral acid treatment showed relatively less yield than organic acid. Higher yields with different neutralization methods have been reported earlier (Yu et al. 2013).

The average hydrodynamic diameter of PCNC, CCNC, and HCNC were observed to be 248.7 ± 1.11 nm, 141.8 ± 2.52 nm, and 128.7 ± 3.24 nm, respectively. Hydrogen peroxide hydrolysis degraded the substrate more uniformly and produced CNC II as long cylinders corresponding to bundles of nanofibrils. Similar effect was observed when CNC was extracted using catalytic peroxide oxidation (Koshani et al. 2018). The particle size analysis of CCNC and HCNC revealed their corresponding hydrodynamic diameter to be 141.8 nm and 128.7 nm, respectively. The smaller particle size is the result of efficient hydrolysis by both organic and mineral acid.

The zeta potential values of CNC provide evidence for the net charges present on the surface of the nanoparticle as function of pH. The charge on the surface determines the dispersion stability of a colloidal system comprising of CNC. Colloidal solution with zeta potentials less than −30 mV and more than +30 mV could maintain a stable system due to repelling forces between particles (Lin et al. 2019). The charges are result of type of hydrolyzing method employed to extract CNC. The peroxide and citric acid treatment is expected to attach carboxylate group to the CNC surface. The zeta potential value for PCNC and CCNC were found to be −23 ± 0.34 mV and −19.9 ± 0.87 mV, respectively. The value of PCNC was found closer to the value of carboxylated CNC prepared by APS oxidation (Cheng et al. 2014). Similar values were observed when carboxylated CNCs, which were obtained using iron catalyzed peroxide hydrolysis (Fan et al. 2019). The lowest zeta potential value was observed for CCNC (−19.9 mV). The low value indicates the lower content of carboxylic groups that were created by esterification of hydroxyl groups of CNC (Nagarajan et al. 2020). The previous reports, however, presented CNC with higher zeta potential values (in the range of 90–123 mV) when only citric acid was used (Ji et al. 2019) and when mixture of citric and hydrochloric acid was used, the value ranged between −33 mV and −46 mV (Yu et al. 2016). The zeta potential of HCNC was −24.9 ± 0.23 mV, which is comparatively better values than that of CNC obtained using hydrothermal hydrochloric acid-based hydrolysis followed by different neutralization techniques (Yu et al. 2013). Zeta potential for lignin-CNC II extracted using alkaline pulping and acidic hydrolysis from cedarwood sawdust and beech sawdust was observed to be −18.9 mV and −21.7 mV, respectively (Hajam et al. 2022). The lack of surface charge creation by hydrochloric acid method is usually considered a drawback compared to conventional sulfuric acid method, as it could lead to aggregation of CNCs, thereby resulting in

poor colloidal stability. The zeta potential values of HCNC suggested moderate to good dispersion stability. CNCs with good stability will enhance its applicability in a variety of applications ranging from wastewater treatment to composite reinforcement.

Morphological characterization

The microstructural characteristics of the prepared CNCs were observed using FE-SEM, and the micrographs are given in Fig. 2a-c (low magnification) and Fig. 2a–c (high magnification). The CNC samples exhibited typical rod-like morphology with high length to diameter ratio. Citric acid treatment rendered CNC with thin needle-like morphology (Fig. 2B). This was due to the acid penetrating the amorphous region of cellulose, leaving the ordered crystalline nanoparticles in longitudinal direction (Ji et al. 2019). These needle-shaped nanoparticle tend to form web-like structures that had enhanced physical properties of composite films reported recently (Lu et al. 2021). The rod-like structure of obtained CNC confirmed the efficiency of the mild extraction methods that resulted in highly crystalline entities (Yu et al. 2013).

The prepared cellulose II nanocrystal suspension (0.1 wt%) exhibited a colloidal state when observed under ambient light conditions (Fig. 3). The transmittance of PCNC, CCNC, and HCNC was found to be 71.13%, 74.06%, and 69.5% at 600-nm wavelength, respectively. The translucent appearance of colloidal suspension well reflected in the UV-Vis spectrometer. The findings were identical to the cellulose II nanocrystal suspension prepared from sulfuric acid hydrolysis of eucalyptus cellulose (Xing et al. 2020).

Crystallography of CNC

The XRD pattern of pretreated cellulose pulp, PCNC, CCNC, and HCNC is given in Fig. 4a. All samples exhibit key diffraction peaks at 2θ ≈ 12.2°, 20°, and 21.7° corresponding to 1–10, 110, and 020 planes, respectively. These are the characteristic peaks for cellulose type II polymorph (Gong et al. 2017; Lu et al. 2021). The intense double peak in CNCs compared to that of pretreated pulp confirms the efficiency of extraction methods in hydrolyzing the amorphous regions, leaving out the rigid crystalline region. The crystallinity index and crystallite size of the CNCs are given in Table 1. The crystallinity (CrI) of pretreated pulp, PCNC, CCNC, and HCNC were found to be 62%, 81.1%, 75.4%, and 86.1%, respectively. The crystallinity of PCNC is high and close to the CNCs prepared using catalytic oxidation using peroxide (Koshani et al. 2018) and that of the ones prepared using conventional acid hydrolysis from bleached soft wood kenaf (Li et al. 2011). The CrI of CCNC was comparatively lower than other two methods. This could be because of
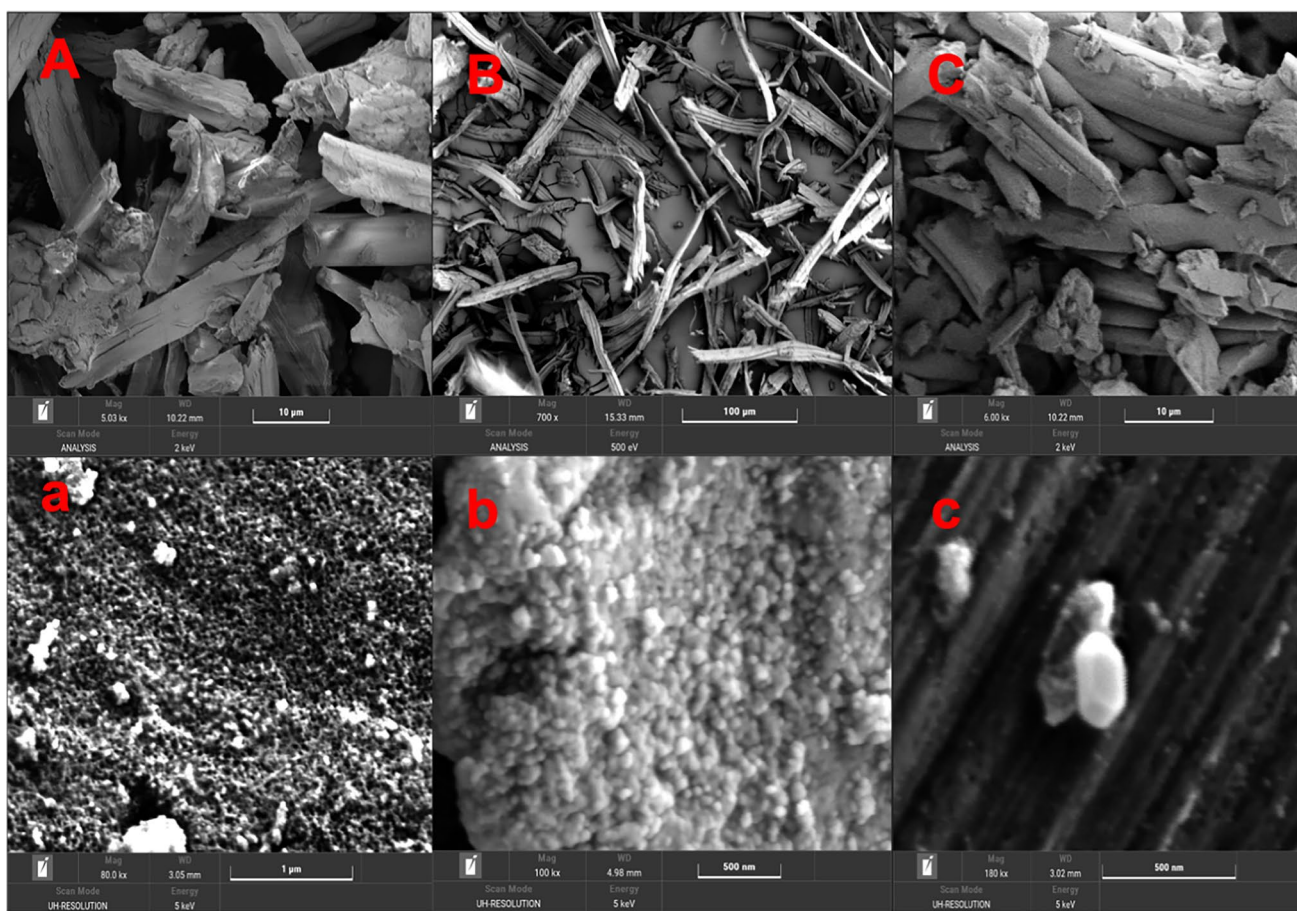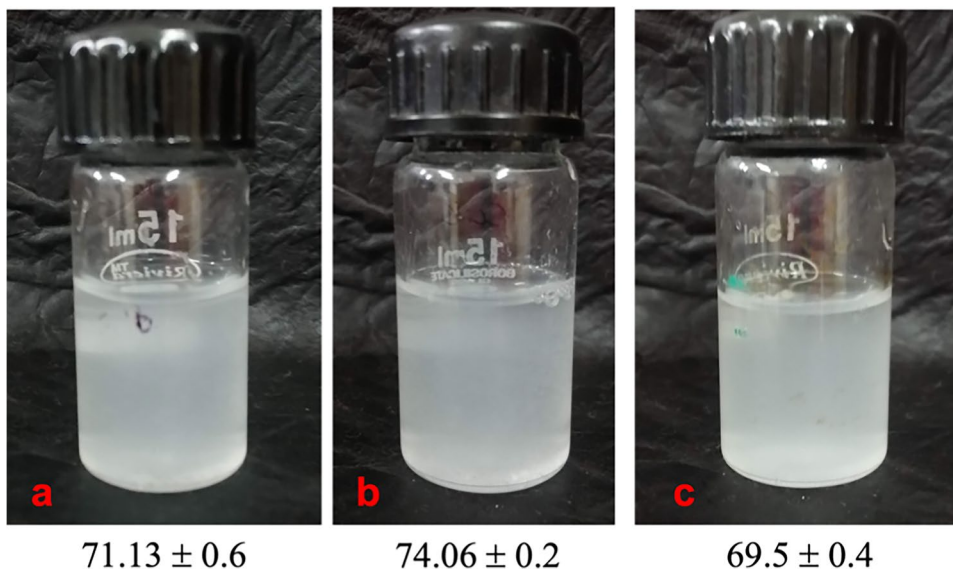
Fig. 2 FE-SEM micrographs of cellulose II nanocrystals prepared by different techniques presented at different levels of magnification

Fig. 3 Light transmittance of CNC II suspension (**a**) PCNC, (**b**) CCNC, (**c**) HCNC

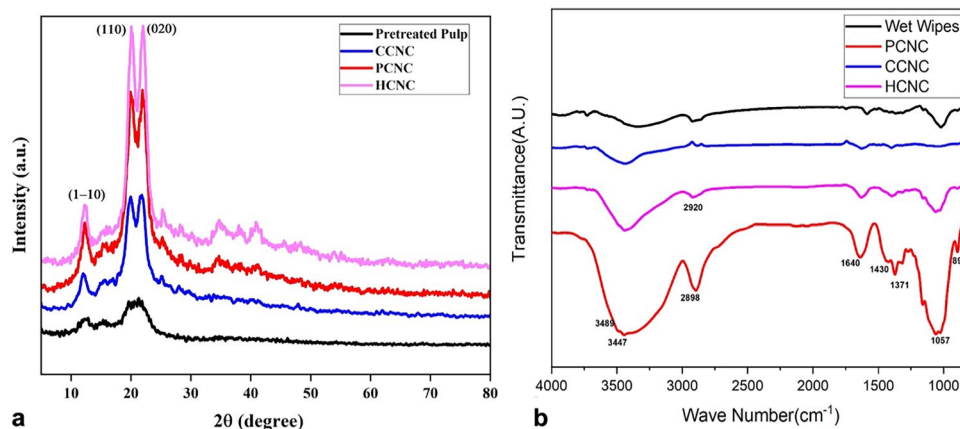$$71.13 \pm 0.6 \qquad 74.06 \pm 0.2 \qquad 69.5 \pm 0.4$$

carboxylic acid released during the reaction between citric acid and cellulose, which affected some of the crystalline region too (Nagarajan et al. 2020). The HCNC were prepared with high order of crystallinity. Hydrochloric acid is less aggressive than sulfuric acid, thus attacks crystalline region less, just as in the case with other mild acids (Yu et al.

Fig. 4 a X-Ray diffractogram of cellulose II nanocrystals; **b** FTIR spectra of CNC II and wet wipes

of OH groups that emanated from hydrogen bond breaking during peroxide oxidation reaction (Koshani et al. 2018).

The crystallinity of wet wipe cellulose, PCNC, CCNC, and HCNC were calculated using ratio between absorption intensities at crystalline peak and amorphous peak. The CrR values are tabulated in Table 1. The crystallinity of HCNC was found to be maximum (2.565) among the other CNC and wet wipe cellulose. This is in congruence with the observation from X-ray crystallography studies where maximum intensity was observed for HCNC sample. The characteristic features of the prepared cellulose II nanocrystal were compared (marked in bold) with the prevalent literatures and tabulated in Table 2.

Characterization of bio-nanocomposite film

Mechanical characterization of films

Thickness and mechanical performance of all films are given in Fig. 5a–c. The thickness of the films ranged between 150 and 193.34 μm. There was no significant difference in thickness measurements of the films when compared to control gelatin film ($p > 0.05$). The tensile strength of the nanocomposite films had increased with the addition of CNC. The significant improvement in tensile strength values compared to the control gelatin film was observed in GPCNC (50.22% increase) films and GCCNC films (41.89% increase). Generally, cellulose II is more reactive than cellulose I, and more hydrogen bonding interactions are possible (SaifulAzry et al. 2021). The reinforcement of PCNC and CCNC is the result of strong interfacial bonding between gelatin and CNC. The mechanical strength is dependent on the relative volume fractions of hard phase and soft phase. The high crystallinity of CNC makes it rigid and stiff that arrests the mobility of the polymer network. The rod-like nanostructure with high aspect ratio enhanced the stiffness and reduced flexibility of the nanocomposite film, resulting in reduced elongation at break values. Similar kind of results were observed when CNC

2013). The crystallinity of CNC II was found to be higher than the previous reports so far (Mahmud et al. 2019; Lu et al. 2021; SaifulAzry et al. 2021). Pretreated cellulose pulp with lower crystallinity has smaller crystallite size in crystalline region. The crystallite size (CS) of the CNC II were observed to be 4.49 nm, 5.39 nm, and 5.5 nm for PCNC, CCNC, and HCNC, respectively. Cellulose II nanocrystals prepared using sulfuric acid hydrolysis of *Cynara scolymus L.* stems were composed of minute crystals with crystallite size ranging between 5 and 9 nm (Potenza et al. 2022). The values obtained in this work were also found closer to the crystallite size of CNC II as obtained by Jin et al. (2016). The crystallite size of CNC II prepared from medical cotton using 85% phosphoric acid were observed in the range of 10.02 nm and 11.1 nm (Mahmud et al. 2019).

FTIR spectroscopy of cellulose nanocrystal

Figure 4b shows the FTIR spectrographs of wet wipe cellulose, PCNC, CCNC, and HCNC. All the spectrum showed characteristic peaks at around 3600 and 3100 cm^{-1} associated with –OH bond stretching, and peaks near 2900 cm^{-1} indicated C-H stretching vibration. The spectra featured two distinct peaks at 3447 cm^{-1} and 3489 cm^{-1} which are characteristic of cellulose type II polymorph, indicating the intramolecular hydrogen bonds of cellulose II (Huang et al. 2022; Xing et al. 2020). The band at 1640 cm^{-1} and 1371 cm^{-1} is associated with O–H bending of absorbed water and C-H stretching vibration (Huang et al. 2022). The C–O stretching band of pyranose (C_6) unit at 1057 cm^{-1} was also observed (Mahmud et al. 2019). The peak at 1430 cm^{-1} is associated with –CH$_2$ bending vibration of C_6 which is known as "crystallinity" band of cellulose. The 895 cm^{-1} peak corresponds to C–O–C stretching vibration, considered as "amorphous" band, which is indicative of cellulose type II (Lu et al. 2021; Mahmud et al. 2019). The intensified broad band at 3300 cm^{-1} in PCNC is due to the stretching vibration

Table 2 Comparison of characteristics of cellulose (II) nanocrystals

Source		Method of extraction	Yield (%)	CrI (%)	Length (nm)	Reference(s)
Buckeye cellulose		HCl/H$_2$SO$_4$ hydrolysis	33	67	500	Zhang et al. 2007
Bacterial cellulose		SO$_3$/Pyridine in DMAc/LiCl medium	34	69.9	-	Qin et al. 2014
Cellobiose		Cellodextrin phosphorylase from cellulolytic bacterium (*Clostridium spp.*)	-	-	254	Kuga et al. 2022
Commercial cellulose (Avicel PH-101 and Arbocel UFC 100 Bright)		NaOH mercerization (16% solution)	-	43	120	Grzabka-Zasadzinska et al. 2021
Oil palm fronds		Hydrochloric acid hydrolysis	-	47	200	Hussin et al. 2016
Cellulose pulp		NaOH mercerization (16% solution) and H$_2$SO$_4$ hydrolysis (64% solution)	-	-	140	Borysiak and Grzabka-Zasadzinska 2016
Lignocellulosic biomass		NaOH mercerization	67	73	-	Nagarajan et al. 2017
Cedarwood sawdust (softwood)		Alkaline pulping/ bleaching/H$_2$SO$_4$ hydrolysis (64% solution)	-	62.07 (Lignin-CNC) 65.86 (Lignin-free CNC)	87 (Lignin-CNC) 96 (Lignin-free CNC)	Hajam et al. 2022
Beechwood sawdust (hardwood)		Alkaline pulping/ bleaching/H$_2$SO$_4$ hydrolysis (64% solution)	-	75.59 (Lignin-CNC) 79.47 (Lignin-free CNC)	145 (Lignin-CNC) 155 (Lignin-free CNC)	Hajam et al. 2022
Mango seed		H$_2$SO$_4$ hydrolysis (11.21 M solution)	22.8	90.6	123.4	Henrique et al. 2013
Rice husk		Alkaline treatment/ Chlorine- free bleaching/ H$_2$SO$_4$ hydrolysis (64% solution)	45.1	66.19	164	Hafemann et al. 2020
Cynara scolymus L. (Artichoke stem)		H$_2$SO$_4$ hydrolysis (40% solution)	-	63-75	200	Potenza et al. 2022
Wet-wipe cellulose	**PCNC**	**Hydrogen Peroxide hydrolysis**	**66**	**81.1**	**248.7**	**This work**
	CCNC	**Citric acid hydrolysis**	**81**	**75.4**	**141.8**	
	HCNC	**Hydrochloric acid hydrolysis**	**77**	**86.1**	**128.7**	

were used as reinforcement in potato starch–based film and soy protein isolate–based films (Noshirvani et al. 2018; Huang et al. 2020). The increase in tensile strength by CNC could also be due to electrostatic attraction that exists between gelatin (at pH 3) and negatively charged CNC particle (Leite et al. 2021a). The enhancement in mechanical properties by HCNC was not significantly different from the control gelatin film ($p>0.05$). The smaller particle of HCNC dispersed well and increased the homogeneity that imparted not much of a difference in the physical properties.
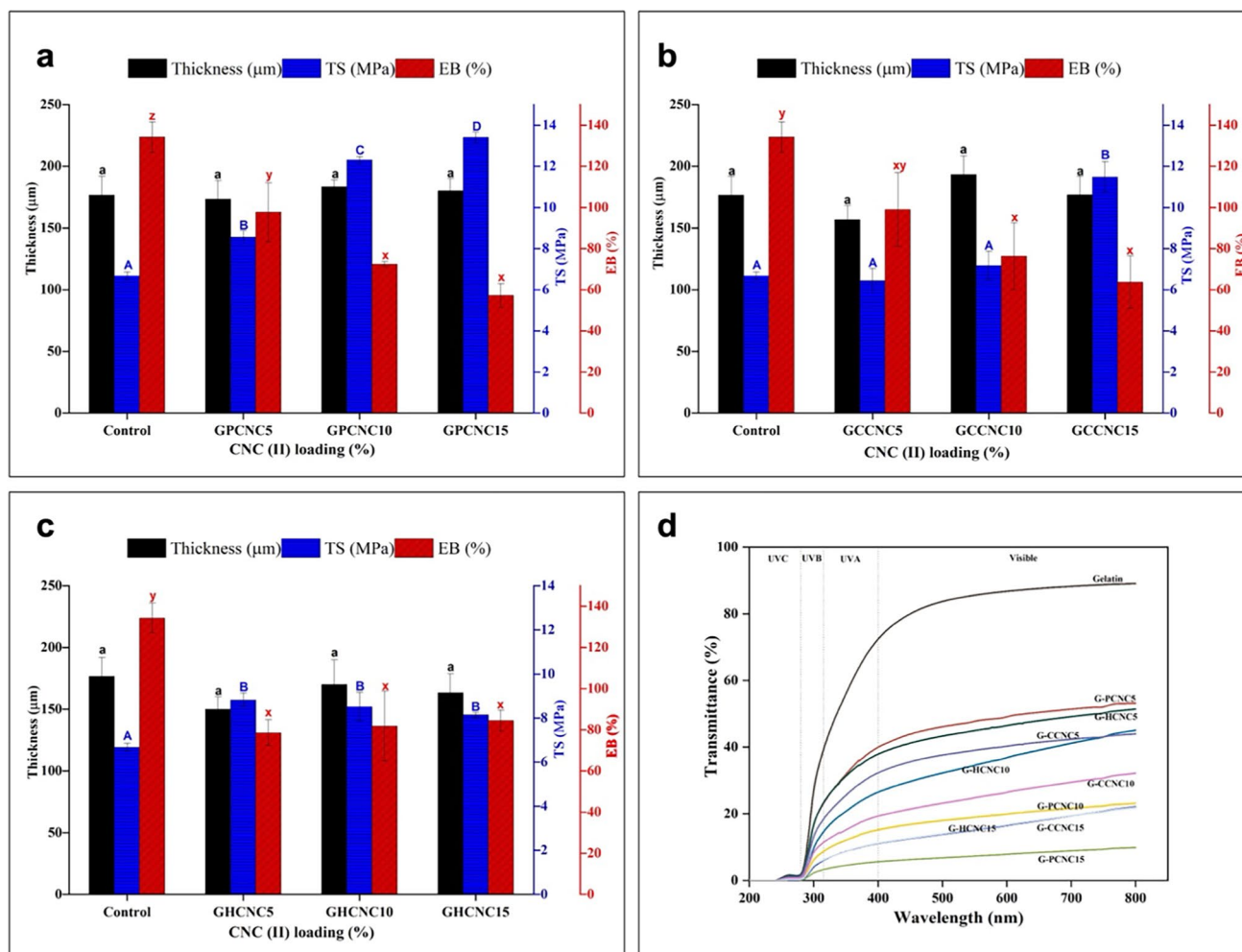
Fig. 5 Mechanical properties of nanocomposite films **a** GPCNC films; and **b** GCCNC films; **c** GHCNC films; **d** UV-Vis transmittance of films (Different alphabets as superscripts in the same column indi-

cate significant differences between mean according to Tukey test (p <0.05). a-c: Thickness; A-C: Tensile strength (TS); x-z: Elongation at break (EB)

Thermal characterization of films

Figure 6a and b represents the TGA thermogram and derivative curve as dTG of control gelatin, GPCNC15, GCCNC15, and GHCNC15 films, respectively. The degradation profile of all the films majorly exhibited three phases. The first phase at around 80–100 °C was related to the evaporation of water and degradation of glycerol from the matrix. There occurs a small weight loss at this stage. The second phase is attributed to cellulose thermal degradation and the temperature at which the decomposition begins is termed as onset temperature (T_o). The onset temperature for control gelatin and nanocomposite films was found to be above 250 °C, indicating good thermal stability. The third phase occurs when maximum decomposition of the matrix occurs, which is marked by the dTG curves. The T_{max} of control gelatin, GPCNC15, GCCNC15, and GHCNC15 was observed to be 317 °C, 329 °C, 318 °C, and 315 °C, respectively. The thermal stability of films reinforced with CNCs were found

to be better than control gelatin film. The CNCs in type II polymorph are inherently thermodynamically stable due to their packing structure (Jin et al. 2016; Wang et al. 2014). Also, higher thermal stability is associated with crystallinity as higher energy is required for thermal decomposition of highly crystalline material (Lu et al. 2021). The results are well in agreement with the crystallography results.

The effect of hydrolysis method of CNC has a significant effect on its thermal stability, which in turn reflects in the nanocomposite film. It is well known that surface-sulfated groups created by sulfuric acid hydrolysis on the anhydroglucose unit require less energy, which could release sulfuric acid at much lower temperature during thermal degradation process. This released sulfuric acid would act as a catalyst in facilitating cellulose decomposition (Yu et al. 2013). The CNC prepared by sulfuric acid hydrolysis would therefore have lower thermal stability (Mahmud et al. 2019; Lei et al. 2018). The current work utilizes peroxide, citric acid, and hydrochloric acid to extract CNC, which were beneficial

Fig. 6 **a** TGA; **b** dTG of gelatin-CNC films; **c** DSC thermograms of nanocomposite films; **d** ATR spectrographs of films
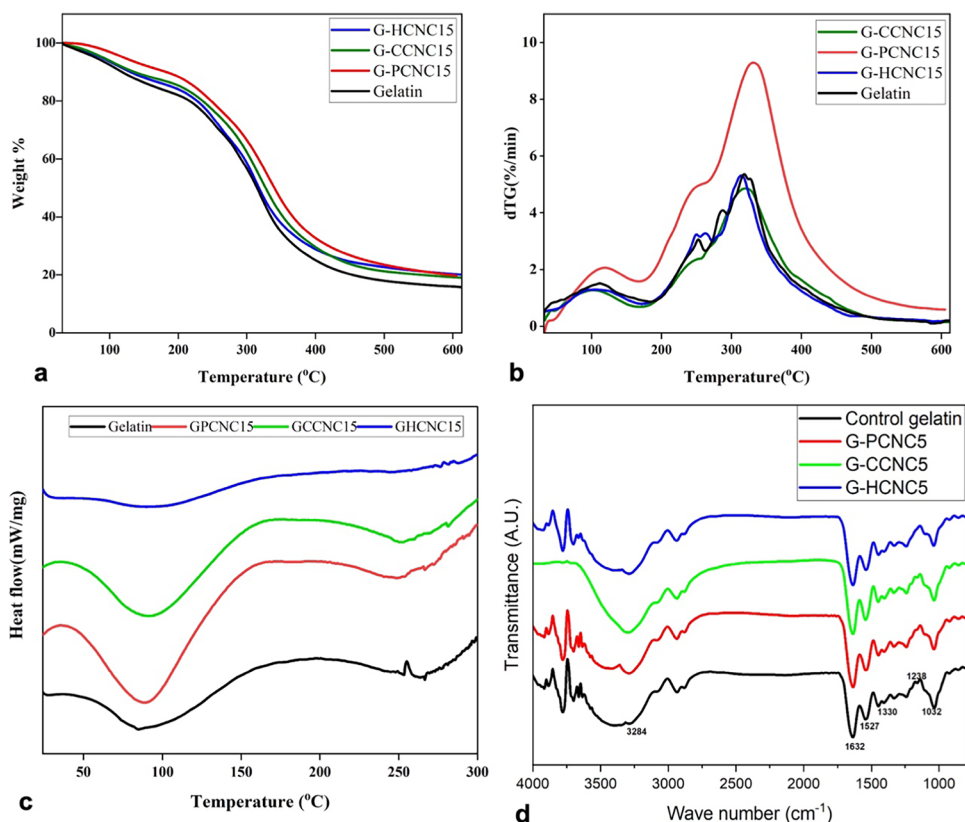
in providing better thermal stability. The char residue of GPCNC15, GCCNC15, GHCNC15, and control gelatin films were observed to be 19.71%, 19%, 20.05%, and 15.8% at the end of thermal degradation process, indicating the enhanced flame resistance exhibited by the CNC-II (Gonzalez-Dominguez et al. 2019). The higher thermal stability offered by CNC in a nanocomposite would widen its scope of applicability in various fields.

Differential Scanning Calorimetry (DSC)

DSC thermograms of control gelatin film and bio-nanocomposite films with 15% CNC II is given in Fig. 6c. The spectra of films exhibited endothermic peaks occurring at around 89–100 °C, which is attributed to water evaporation, and molecular relaxation at such temperature overlapping the T_g of gelatin component (approximated at around 75–80 °C) (Masilamani et al. 2017; Mondragon et al. 2015). This was in line with the observations from TGA. Another endothermic peak at 250 °C is observed for gelatin film and GCCNC15, which is attributed to melting temperature of the composite film caused due to the devitrification of proline and hydroxyproline imino acids. In case of GPCNC15 film, this peak shifted to slightly lower temperature indicating the recrystallization induced by nanocrystals that acted as nucleating agent in protein

films (Hosseini et al. 2015). The changes in temperature in GHCNC15 film was observed to be insignificant.

ATR spectrographs of gelatin-CNC composite films

The ATR-FTIR spectrographs of control gelatin and nanocomposite films are shown in Fig. 6d. The main characteristic peaks were observed at 3500–2300 cm^{-1} corresponding to OH and NH stretching (amide A), 1640 cm^{-1} corresponding C=O stretching (amide I), 1527 cm^{-1} related to N-H bending (amide II), and 1238 cm^{-1} indicating C-N stretching (amide III) (Mondragon et al. 2015). The broad band at 3000 cm^{-1} also corresponded to free and bound OH from water molecule present in the films. The peak 2915 cm^{-1} observed due to stretching of C-H of the cellulose molecule (Sasikala and Umapathy 2018). The peak at 1330 cm^{-1} is attributed to wagging of –CH$_2$ of proline from the gelatin (Uranga et al. 2016). The band at 1032 cm^{-1} is associated with the interactions between glycerol and hydroxyl groups present in the film (Santos et al. 2014). No significant changes in peak intensities were observed between control gelatin and GCNC films indicating the absence of very strong intermolecular modification amongst the polymeric components of the nanocomposite film.

UV-Vis and transparency properties of films

UV-Vis transmittance exhibited by control gelatin film and nanocomposite films are given in Fig. 5d. All films including control gelatin film showed excellent light barrier properties, specifically in UVC (200–280 nm) region. This is due to the presence of chromophore groups such as tyrosine and phenylalanine amino acid groups in gelatin network, which have unsaturated bond that absorb UV radiation (Chuaynukul et al. 2018). Addition of CNC to the gelatin film decreased the light transmittance in both UV and visible light radiation region to a considerable extent. The light transmittance reduced significantly with increase in concentration of CNC II, which is evident from the plot where all films with 15 wt% CNC showed transmittance below 20%. The presence of hydroxyl group from the CNC acts as auxochrome when conjugated with the pre-existing chromophore from the gelatin and absorbs more light (Uranga et al. 2016). The opacity of the films is also dependent on the crystalline character and the particle size of the nanocrystal. The least light transmission observed with GPCNC15 film was due to the high crystallinity and hindrance caused due to agglomeration of PCNC particle at high concentration (Haghighi et al. 2021; Alves et al. 2015). The scattering of light is more at such concentration than reflection. The shielding effect by films with CCNC could be due to few conjugated carboxyl and carbonyl groups formed at the pyranose ring of CNC during citric acid treatment. These group act as chromophores in absorbing light radiation (Yang et al. 2020).

The transparency at 600 nm was calculated and given in Fig. 7a–c. The highest value of transparency (11.27 A mm^{-1}) was obtained for control gelatin film. The value of transparency decreased with increase in CNC concentration ($p < 0.05$). The reduction in light transmission was very small in case of GHCNC films. This indicated the better dispersion of HCNC in gelatin matrix compared to other CNC II nanoparticles. Homogeneity and compatibility between HCNC and gelatin were better, which led to light transmission similar to control gelatin film (Pei et al. 2013).
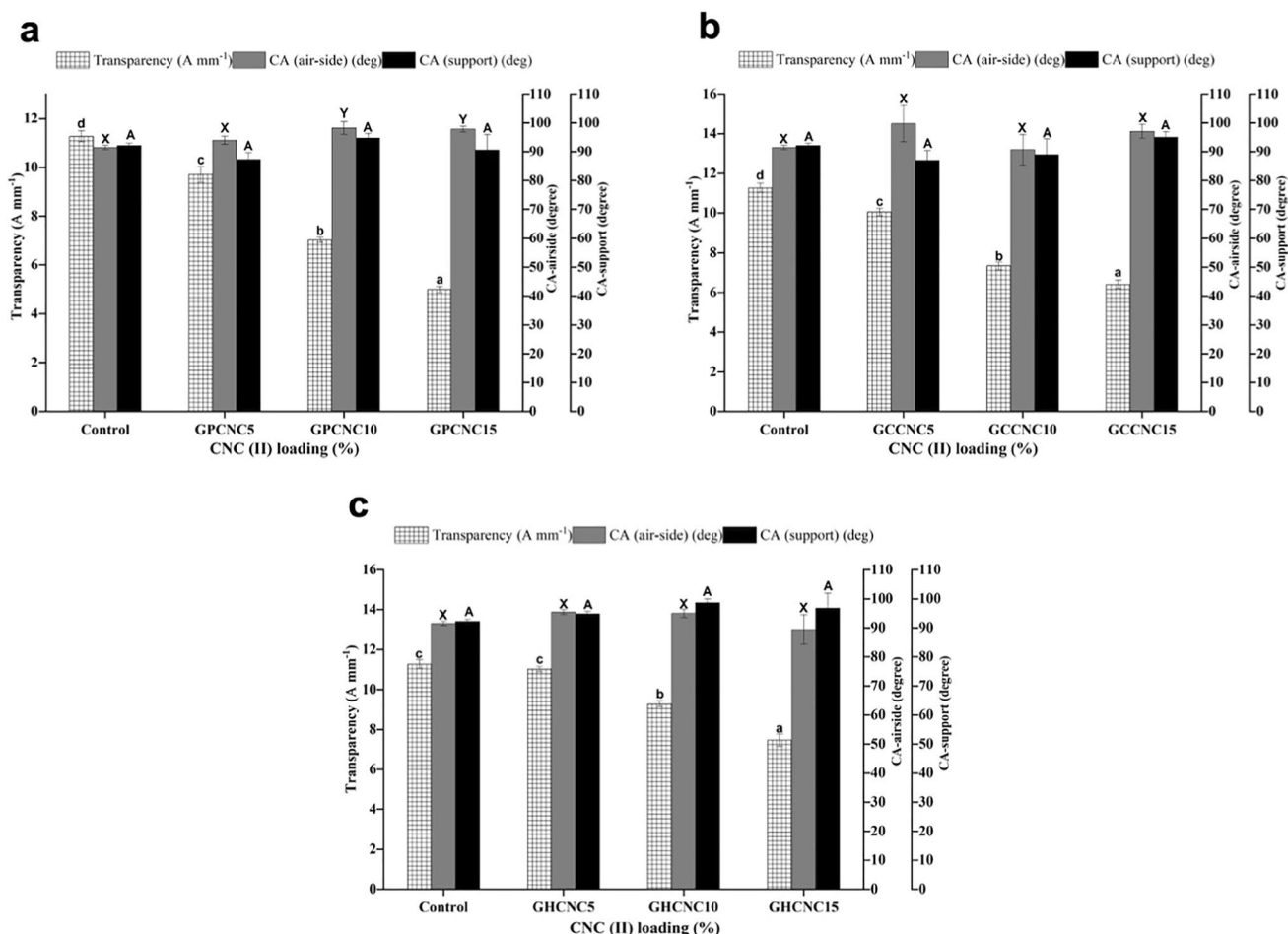
Fig. 7 Transparency and contact angle of films **a** GPCNC; **b** GCCNC; **c** GHCNC. (Different alphabets as superscripts in the same column indicate significant differences between mean according to Tukey test ($p < 0.05$). a-d: Transparency; X-Z: CA (air-side); A-C: CA (support side)

Table 3 Light transmittance of Gelatin-CNC II films

CNC II loading	T_{660} (%)		
	GPCNC	GCCNC	GHCNC
Control		87.8 ± 0.6^d	
5%	50.5 ± 0.7^c	40.78 ± 0.7^c	48.1 ± 0.5^c
10%	20.9 ± 0.08^b	28.04 ± 0.5^b	38.8 ± 0.6^b
15%	8.2 ± 0.3^a	18.2 ± 0.2^a	18.1 ± 0.2^a
CNC II loading	T_{280} (%)		
	GPCNC	GCCNC	GHCNC
Control		1.82 ± 0.06^c	
5%	1.83 ± 0.05^c	1.21 ± 0.04^d	1.74 ± 0.02^c
10%	0.56 ± 0.02^b	0.76 ± 0.04^b	0.62 ± 0.03^b
15%	0.19 ± 0.02^a	0.36 ± 0.02^a	0.34 ± 0.03^a

[*]Mean $\pm$ standard deviation ($n=3$)

[**]Different alphabets as superscripts in the same column indicate significant differences between means, according to Tukey test ($p<0.01$)

Optical light transmittance of nanocomposite films

The light transmittance of nanocomposite films in the UV (280 nm) and visible range (660 nm) is given in Table 3. The light barring character of gelatin films was significantly decreased with increasing nanocrystal concentration ($p<0.01$). GPCNC15 film had the least T_{660} value of 8.2%. The UV barrier capability was found to be excellent for all composite films with T_{280} values below 2%. Addition of nanocrystals improved the UV barrier further, rendering the GPCNC15 film with the most UV blocking capacity with a value of 0.19%. These values were better than the food packaging carrageenan films reinforced with TiO_2 nanotubes resulting in UV transmittance of 9.1% and visible light transmittance of 31.1% (Ezati et al. 2021). Light blocking including UV is a key requirement for packaging materials, as light could cause photodecomposition of food, oxidation, and rancidity of the packed food material reducing its viability for consumption. The prepared nanocomposite films are beneficial as packaging materials with such outstanding UV and light barrier characteristics.
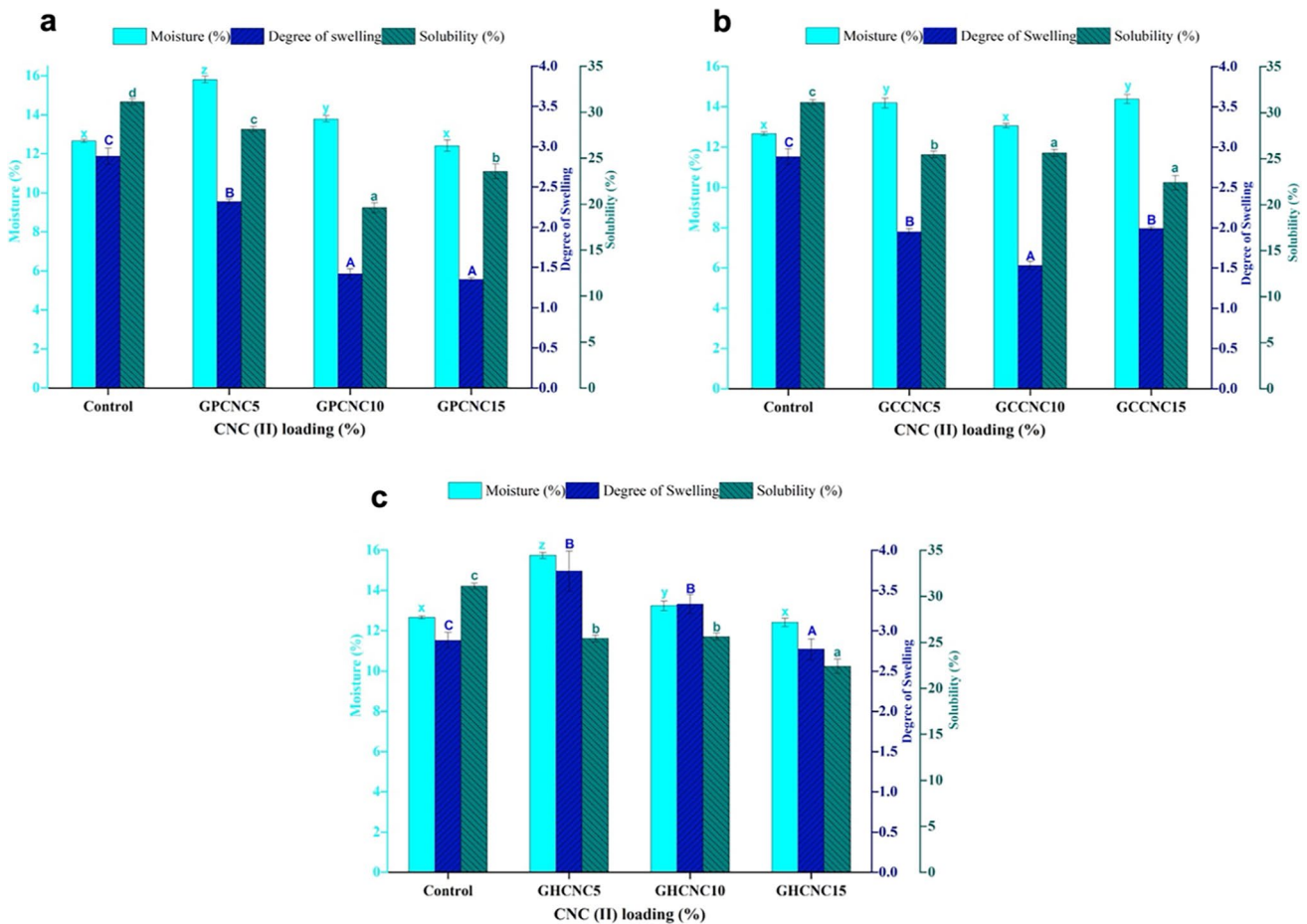
Fig. 8 Moisture sensitivity of films **a** GPCNC; **b** GCCNC; **c** GHCNC. (Different alphabets as superscripts in the same column indicate significant differences between mean according to Tukey test ($p <0.05$). x-z: Moisture content; A-C: Degree of swelling; a-d: Solubility

Moisture sensitivity of films

Moisture sensitivity, evaluated with the help of moisture content, degree of swelling, and solubility of films, in aqueous environment is given in Fig. 8. The moisture content of the films ranged between 12.47 and 15.81%. The inherent moisture content was slightly higher for films with lower concentration of CNC in all three cases, when compared to control gelatin films. The detectable moisture level decreased with increase in CNC concentration. This could be attributed to the presence of higher amounts of water-insoluble cellulose nanocrystal in the gelatin matrix.

Degree of swelling represents the moisture uptake by the nanocomposite films. Moisture resistance by the GPCNC and GCCNC films were observed to be better than the control gelatin film. At lower concentrations, the strong interfacial adhesion between the cellulose nanocrystal and the polar group of gelatin prevented moisture absorption. The agglomeration of the CNC at high concentration did not result in significant improvement in moisture uptake. Similar trend of result was observed when CNC prepared from garlic stalks were used as reinforcement in starch-based biopolymer film (Agustin et al. 2013).

Solubility of nanocomposite films was found to be lower than that of control gelatin films. The reduction of solubility at lower loading levels of CNCs was evident from Fig. 8. Such improvement is due to the Gel-CNC complex coacervate formation that occurred with gelatin being present at around pH 3. This complexation resulted in reduced charged interactions which decreased solubility (Leite et al. 2021a). The strong hydrogen bond formation between the hydroxyl groups and polar groups of the gelatin created three-dimensional network limiting the mobility of the water molecule, thereby reducing the solubility (Noshirvani et al. 2018; Xiao et al. 2021). Amorphous regions of CNC are more prone to moisture absorption than crystalline region. With use of highly crystalline nanocellulose, improvement in moisture sensitivity was inevitable (Pereira et al. 2017).

Water Contact angle

The contact angle measurements on the either side of the nanocomposite film depicts the wettability of the surface (Fig. 7). The "air side" of the film represents the exposed side of the film from the petri dish, whereas the "support side" denotes the side attached to the petri dish. The control gelatin film exhibited contact angle above 90°, despite the hydrophilic character of the polymeric matrix. Incorporation of CNC improved the hydrophobicity of the films. The differences in the water contact angle values on either side of the films were predominantly observed in the case of GPCNC films. This could be due to the comparatively bigger sized nano-rod CNC that formed an interconnected

pseudo bilayer on the surface of the film, which created a rough surface on one side. Rough surfaces modulate the contact angle as they contain air fractions that prop up water droplet from the surface increasing the water contact angle. Such rough surfaces can exhibit better hydrophobicity and may increase the tortuosity for water molecules making the film water impermeable. It was demonstrated in literature that assembly of hydrophilic nanocellulose and nano-clay surfaces led to increased water contact angle (Wu et al. 2014).

In case of GHCNC films, the dispersion of CNC within gelatin network was better and no significant improvement in water contact angles were observed when compared to control gelatin films ($p > 0.05$). The results were in line with the observations from light transmission experiment. The strong hydrogen bonding interaction between hydroxyl group of highly crystalline CNC and gelatin contributed to improved wettability characteristics (Noshirvani et al. 2018; Coelho et al. 2020). Similar trend of results was observed when bovine gelatin was reinforced with 2.5% CNC that improved water contact angle value to 95.2° from 80.7° for control gelatin film (Leite et al. 2020).

Antimicrobial activity of nano-biocomposite films

The antibacterial activity against foodborne pathogens, *S. aureus* (Gram-positive bacteria) and *E.coli* (Gram-negative bacteria), by the nanocomposite film discs with lowest (5%) and highest (15%) CNC II loadings are depicted in Fig. 9. Growth inhibitory zones around films P5 (GPCNC5), C5 (GCCNC5), P15 (GPCNC15), and C15(GCCNC15) were observed in *S. aureus* growth MHA plates with G (gelatin) films dissolving and drained around the growth. Sample discs H5 (GHCNC5) and H15 (GHCNC15) were not structurally stable and found to be contracted within incubation duration (Fig. 9a and b). However, there was no inhibitory effects observed against *E. coli* by the nanocomposite film samples, albeit with a similar draining effect by the control gelatin sample. The zone of inhibition was exhibited by the films against Gram-positive *S. aureus* but not against Gram-negative *E.coli* bacteria. This is explained by the difference in the cell wall structure of the Gram-negative bacteria, which prohibits several molecules from crossing its triple-layered thick membrane, whereas Gram-positive bacteria lacks such membrane thereby allowing the passage (Perumal et al. 2022). According to the Standard SNV 195920-1992, antibacterial effect of material is considered "good" when inhibition zone is observed under and around the samples and considered "sufficient" when inhibition area is formed only under the sample (Leite et al. 2021b). Hence, the films are found to be suitable for sustainable packaging applications with sufficient antibacterial activity.

Fig. 9 Antibacterial activity of nanocomposite film discs against **a** and **b** *S. aureus* and **c** and **d** *E.coli* with different CNC II loadings
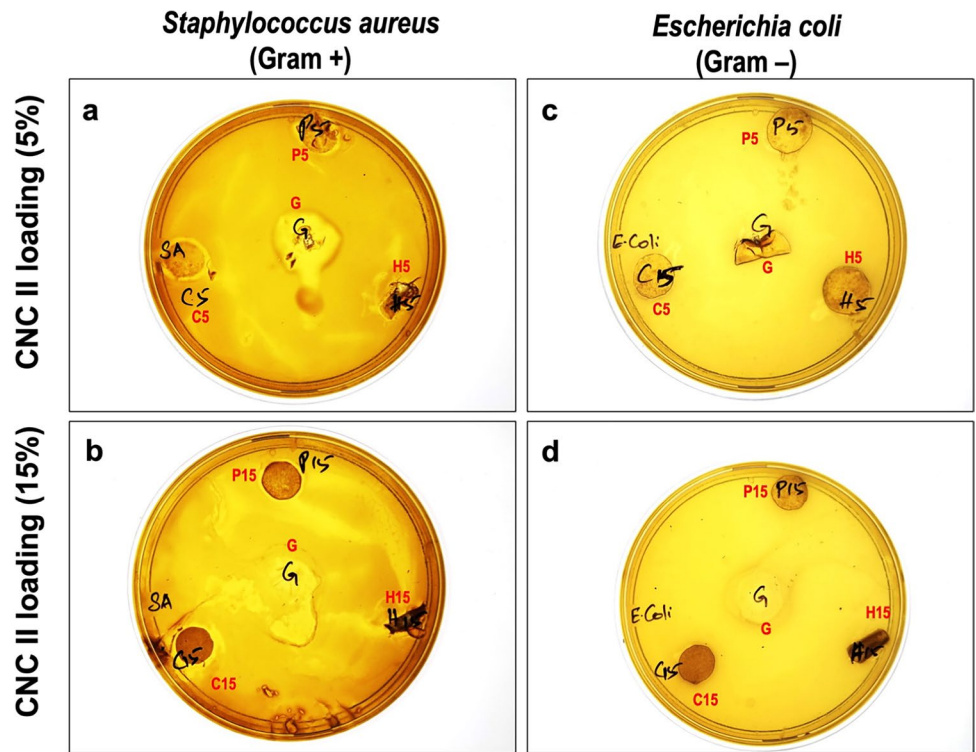
Fig. 10 Visual degradation profile of nanocomposite films under soil burial degradation
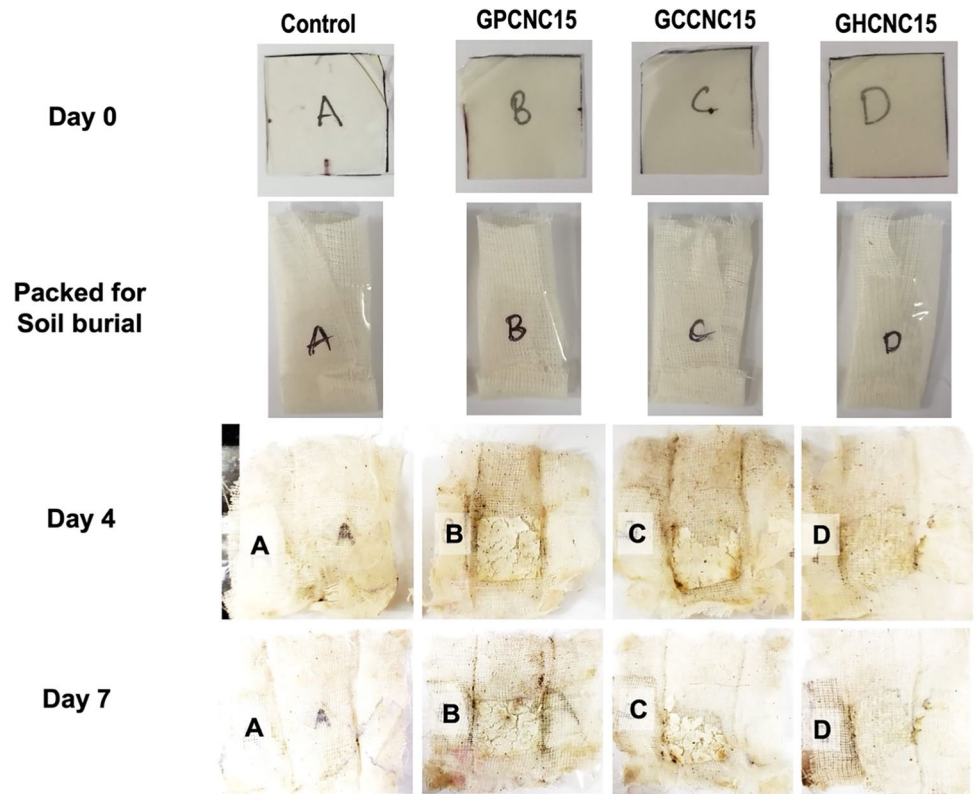
Biodegradation of films

The control gelatin film (A) and nanocomposite films (B, GPCNC15; C, GCCNC15; D, GHCNC15) of size 2 × 2 cm weighing 99.35 mg, 95.35 mg, 95.74 mg, and 102.08 mg, respectively, were buried under soil and observed for a week (Fig. 10). These films were packed in a gauze cloth pocket for better aeration. The control gelatin film was completely degraded within 4 days of soil burial. The nanocomposite films were found to be crumbling, and majority of the degradation happened due to dissolution of gelatin from the films. After a week, the integrity of cellulose network was lost and the weight loss percentage of samples B, C, and D was found to be 61.18%, 71.8% and 79.9%, respectively. With faster rate of biodegradation, these bio-resourced films could best suit single-use plastic application with potential environmental benefits. Similar rate of biodegradation was observed for pigskin gelatin, chitosan, and sodium caseinate–based composite film which disintegrated under composting conditions (Bonilla and Sobral 2020).

Packaging potential of films

Single-use plastic packaging elevates the plastic pollution with its short lifetime and eternal existence without degradation. Packaging applications requiring storage of products under dry, cool conditions could utilize nanocomposite films prepared in this study. The packaging potential of nanocomposite film GPCNC15 as against control gelatin film as eggplant garden seed packaging is demonstrated in Fig. 11. The garden seeds are typically packed in a plastic packaging that keeps the seed dry and viable. Viability of seeds depend on several factors including moisture content, relative humidity and temperature of storage, air permeability, and quality of seeds. The GPCNC15 film was chosen based on the high UV and light blocking capability with high water contact angle. GPCNC15 packet was observed to be dry to touch

when compared to gelatin films. Both control gelatin and GPCNC15 film exhibited better sealing under heat application. Despite the low transparency of the chosen nanocomposite film, the visibility of the seeds through the packaging was not much affected. In addition to the advantage of preserving the viability of the seeds for longer period, the films when discarded in soil along with the seeds could act as fertilizer due to the high protein content from the gelatin biopolymer. Biodegradation profile of GPCNC15 suggests that release of gelatin occurs within 4 days of soil burial. Thus, such strategy of packaging could benefit without any secondary waste generation.

Conclusions

Tannery waste–based gelatin composite films were prepared with cellulose II nanocrystal reinforcement at various concentrations ranging from 5 to 15%. Cellulose II nanocrystal (CNC II) was isolated from wet wipe cellulose using hydrogen peroxide, citric acid, and hydrochloric acid–based hydrolysis techniques, and the effect of hydrolysis technique on morphological and crystalline character of the CNC was evaluated using FE-SEM, XRD, and FT-IR spectroscopy. High yields of CNC II in rod-like nanostructures with high crystallinity index ranging between 75.4 and 86.1% were obtained using the adopted hydrolysis techniques, within a lesser number of purification steps. PCNC and CCNC reinforcement improved the mechanical properties of gelatin films. Highly reactive and crystalline CNC II addition imparted mechanical stiffness and strength. The thermal stability of films was improved owing to the stable cellulose II nanocrystal incorporation. The UV and visible light barrier properties of films with PCNC were found to be maximum, enabled with the three-dimensional network formed by rod-sized nanoparticle on the surface of film. Moisture sensitivities were better for films with PCNC and CCNC than with the mineral acid

Fig. 11 Packaging performance of nanocomposite films **a** control gelatin; **b** GPCNC15

HCl–hydrolyzed CNCs. Rough surface created by PCNC nanorods created hydrophobic surface on one side with water contact angle values of 98° and found to be sufficiently antibacterial against *S. aureus*. Biodegradation of nanocomposites showed that the films decompose maximum within 7 days of soil burial. Single-use packaging application for eggplant seeds has been demonstrated with GPCNC15 films. Further studies are required to evaluate cost-efficient production strategies and scale-up capabilities of the developed packaging films.

Author contribution Vimudha Muralidharan: Conceptualization, Methodology, data curation, software, investigating, writing (original draft), writing (review and editing). Saiprasad Gochhayat: Data curation, methodology, investigating, writing—review and editing. Saravanan Palanivel: Validation, formal analysis, supervision, resources. Balaraman Madhan: Supervision, visualization, validation, project administration, resources, writing—review and editing.

Data availability All data generated and analyzed during this study are included in this article

Declarations

Ethics approval and consent to participate All the authors have given their consent to participate in this publication.

Consent for publication Consented.

Competing interests The authors declare no competing interests.

References

Agustin MB, Ahmmad B, De Leon ERP, Buenaobra JL, Salazar JR, Hirose F (2013) Starch-based biocomposite films reinforced with cellulose nanocrystals from garlic stalks. Polym Compos 34(8):1325–1332

Alves JS, Reis KCD, Menezes EGT, Pereira FV, Pereira J (2015) Effect of cellulose nanocrystals and gelatin in corn starch plasticized films. Carbohydr Polym 115:215–222

Andonegi M, Heras KL, Vizcaino ES, Igartua M, Hernandez RM, de la Caba K, Guerrero P (2020) Structure-properties relationship of chitosan/collagen films with potential for biomedical applications. Carbohydr Polym 237:116159

ASTM-D1746-03 (2003) Standard test method for transparency of plastic sheeting. In: Annual book of American Standards testing methods. American Society for Testing & Materials, West Conshohocken

Beltramino F, Roncero MB, Vidal T, Torres AL, Valls C (2015) Increasing yield of nanocrystalline cellulose preparation process by a cellulase pretreatment. Bioresour Technol 192:574–581

Bonilla J, Sobral PJA (2020) Disintegrability under composting conditions of films based on gelatin, chitosan and/or sodium caseinate containing boldo-of-Chile leaf extract. Int J Biol Macromol 151:178–185

Borysiak S, Grzabka-Zasadzinska A (2016) Influence of the polymorphism of cellulose on the formation of nanocrystals and their application in chitosan/nanocellulose composites. J Appl Polym Sci 133:42864

Briain OO, Mendes ARM, McCarron S, Healy MG, Morrison L (2020) The role of wet wipes and sanitary towels as a source of white microplastic fibres in the marine environment. Water Res 182:116021

Chen L, Zhu JY, Baez C, Kitin P, Elder T (2016) Highly thermal stable and functional cellulose nanocrystals and nanofibrils produced using fully recyclable organic acids. RSC Green Chem 18(13):3835–3843

Cheng M, Qin Z, Liu Y, Qin Y, Li T, Chen L, Zhu M (2014) Efficient extraction of carboxylated spherical cellulose nanocrystals with narrow size distribution through hydrolysis of lyocell fibers using ammonium persulfate as an oxidant. RSC J Mater Chemi A 2:251–258

Chuaynukul K, Nagarajan M, Prodpran T, Benjakul S, Songtipya P, Songtipya L (2018) Comparative characterization of bovine and fish gelatin films fabricated by compression moulding and solution casting methods. J Polym Environ 26(3):1239–1252

Coelho CCS, Silva RBS, Carvalho CWP, Rossi AL, Teixeira JA, Silva OF, Cabral LMC (2020) Cellulose nanocrystals from grape pomace and their use for the development of starch-based nanocomposite films. Int J Biol Macromol 159:1048–1061

De D, Sai MSN, Aniya V, Satyavathi B (2021) Strategic biorefinery platform for green valorization of agro-industrial residues: a sustainable approach towards biodegradable plastics. J Clean Prod 290:125184

Du H, Liu W, Zhang M, Si C, Zhang X, Li B (2019) Cellulose nanocrystals and cellulose nanofibrils based hydrogels for biomedical applications. Carbohydr Polym 209:130–144

Ezati P, Riahi Z, Rhim JW (2021) Carrageenan-based functional films integrated with CuO-doped titanium nanotubes for active food packaging applications. ACS Sustain Chem Eng 9:9300–9307

Fan X-M, Yu H-Y, Wang D-C, Mao Z-H, Yao J, Tam KMC (2019) Facile and green synthesis of carboxylated cellulose nanocrystals as efficient adsorbents in wastewater treatments. ACS Sustain Chem Eng 7(21):18067–18075

FAO (2013) World statistical compendium for raw hides and skins, leather and leather footwear. 1993–2012

George J, Siddaramaiah (2012) High performance edible nanocomposite films containing bacterial cellulose nanocrystals. Carbohydr Polym 87:2031–2037

Geyer R, Jambeck JR, Law KL (2017) Production, use and fate of all plastics ever made. Sci Adv 3:1–5

Gong J, Li J, Xu J, Xiang Z, Mo L (2017) Research on cellulose nanocrystals produced from cellulose sources with various polymorphs. RSC Adv 7:33486

Gonzalez-Dominguez JM, Anson-Casaos A, Grasa L, Abenia L, Salvador A, Colom E, Mesonero JE, Garcia-Bordeje JE, Benito AM, Maser WK (2019) Unique properties and behavior of non-mercerized type II cellulose nanocrystals as carbon nanotube biocompatible dispersants. Biomacromolecules 20:3147–3160

Grzabka-Zasadzinska A, Ratajczak I, Krol K, Wozniak M, Borysiak S (2021) The influence of crystalline structure of cellulose in chitosan-based biocomposites on removal of Ca (II), Mg (II), Fe (III) ion in aqueous solutions. Cellulose 28:5745–5759

Hafemann E, Battisti R, Bresolin D, Marangoni C, Machado RAF (2020) Enhancing chlorine-free purification routes of rice husk biomass waste to obtain cellulose nanocrystals. Waste Biomass Valoriz 11:6595–6611

Haghighi H, Gullo M, China SL, Pfeifer F, Seisler HW, Licciardello F, Pulvirenti A (2021) Characterization of bio-nanocomposite films based on gelatin/polyvinyl alcohol blend reinforced with bacterial cellulose nanowhiskers for food packaging applications. Food Hydrocoll 113:106454

Hajam ME, Kandri NI, Zerouale A, Wang X, Gustafsson J, Wang L, Makila E, Hupa L, Xu C (2022) Lignocellulosic nanocrystals from sawmill waste as biotemplates for free-surfactant synthesis of photocatalytically active porous silica. ACS Appl Mater Interfaces 14(17):19547–19560

Henrique MA, Silverio HA, Neto WPF, Pasquini D (2013) Valorization of an agro-industrial waste, mango seed, by the extraction and characterization of its cellulose nanocrystals. J Environ Manag 121:202–209

Hosseini SF, Rezaei M, Zandi M, Farahmandghavi F (2015) Fabrication of bio-nanocomposite films based on fish gelatin reinforced with chitosan nanoparticles. Food Hydrocoll 44:172–182

Huang S, Tao R, Ismail A, Wang X (2020) Cellulose nanocrystals derived from textile waste through acid hydrolysis and oxidation as reinforcement agent of soy protein film. Polymers 12:958

Huang C, Yu H, Abdalkarim SYH, Li CX, Yang X, Zhou Y, Zhang L (2022) A comprehensive investigation on cellulose nanocrystals with different crystal structures from cotton via an efficient route. Carbohydr Polym 276:118766

Hussin MH, Pohan NA, Garba ZN, Kassim MJ, Rahim AA, Brosse N, Yemloul M, Fazita MRN, Haafiz MKH (2016) Physicochemical of microcrystalline cellulose from oil palm fronds as potential methylene blue adsorbents. Int J Biol Macromol 92:11–19

Ji H, Xiang Z, Qi H, Han T, Pranovich A, Song T (2019) A strategy towards one step preparation of carboxylic cellulose nanocrystals and nanofibrils with high yield, carboxylation and highly stable dispersibility using innocuous citric acid. RSC Green Chem 21(8):1956–1964

Jiang F, Esker AR, Roman M (2010) Acid-catalyzed and solvolytic desulfation of H_2SO_4-hydrolyzed cellulose nanocrystals. Langmuir 26(23):17919–17925

Jin E, Guo J, Yang F, Zhu Y, Song J, Jin Y, Rojas OJ (2016) On the polymorphic and morphological changes of cellulose nanocrystals (CNC-I) upon mercerization and conversion to CNC-II. Carbohydr Polym 143:327–335

Kandasamy R, Venkatesan SK, Uddin MI, Ganesan S (2020) Anaerobic biovalorization of leather industry solid waste and production of high value-added biomolecules and biofuels. In: Rathinam NK, Sani R (eds) Biovalorisation of wastes to renewable chemicals and biofuels. Elsevier, The Netherlands, pp 3–25

Koshani R, Van de Ven TGM, Madadlou A (2018) Characterization of carboxylated cellulose nanocrystals isolated through catalyst-assisted H_2O_2 oxidation in a one-step procedure. J Agric Food Chem 66:7692–7700

Kuga T, Sunagawa N, Igarashi K (2022) Enzymatic synthesis of cellulose in space: gravity is a crucial factor for building cellulose II gel structure. Cellulose 29:2999–3015

Lei W, Fang C, Zhou X, Yin Q, Pan S, Yang R, Liu D, Ouyang Y-K (2018) Cellulose nanocrystals obtained from office wastepaper and their potential application in PET packaging materials. Carbohydr Polym 181:376–385

Leite LSF, Ferreira CM, Correa AC, Moreira FKV, Mattoso LHC (2020) Scaled-up production of gelatin-cellulose nanocrystal bionanocomposite films by continuous casting. Carbohydr Polym 238:116198

Leite LSF, Moreira FKV, Mattoso LHC, Bras J (2021a) Electrostatic interactions regulate the physical properties of gelatin-cellulose

nanocrystals nanocomposite films intended for biodegradable packaging. Food Hydrocoll 113:106424

Leite LSF, Pham C, Bilatto S, Azeredo HMC, Cranston ED, Moreira FK, Mattoso LHC, Bras J (2021b) Effect of tannic acid and cellulose nanocrystals on antioxidant and antimicrobial properties on gelatin films. ACS Sustain Chem Eng 9:8539–8549

Li W, Wang R, Liu S (2011) Nanocrystalline cellulose prepared from softwood kraft pulp via ultrasonic-assisted acid hydrolysis. Bioresources 6:4271–4281

Li N, Bian H, Zhu JY, Ciesielski PN, Pan X (2021) Tailorable cellulose II nanocrystals (CNC II) prepared in mildly acidic lithium bromide trihydrate (MALBTH). RSC Green Chem 23:2778

Lin L, Gu Y, Cui H (2019) Moringa oil/ chitosan nanoparticles embedded gelatin nanofibers for food packaging against *Listeria monocytogenes* and *Staphylococcus aureus* on cheese. Food Packag Shelf Life 19:86–93

Liu WL, Guoying YW, Qin W (2011) Protein-based adhesive prepared from raw material of waste slag from leather making, and preparation method thereof. Patent No.: CN102358830A, China

Lu Q-L, Wu J, Li Y, Huang B (2021) Isolation of thermostable cellulose II nanocrystals and their molecular bridging for electroresponsive and pH-sensitive bio-nanocomposite. Ind Crop Prod 173:114127

Luchese CL, Rodrigues RB, Tessaro IC (2021) Cassava starch-processing residue utilization for packaging development. Int J Biol Macromol 183:2238–2247

Mahmud MM, Perveen A, Jahan RA, Matin MA, Wong SY, Li X, Arafat MT (2019) Preparation of different polymorphs of cellulose from different acid hydrolysis medium. Int J Biol Macromol 130:969–976

Mansikkamaki P, Lahtinen M, Rissanen K (2007) The conversion of cellulose I to cellulose II in NaOH mercerization performed in alcohol-water systems: an X-ray powder diffraction study. Carbohydr Polym 68(1):35–43

Masilamani D, Srinivasan V, Ramachandran KR, Gopinath A, Madhan B, Palanivel S (2017) Sustainable packaging materials from tannery trimming solid waste: a new paradigm in wealth from waste approaches. J Clean Prod 164:885–891

Mondragon G, Pena-Rodriguez C, Gonzalez A, Eceiza A, Arbelaiz A (2015) Bionanocomposites based on gelatin matrix and nanocellulose. Eur Polym J 62:1–9

Moran JI, Alvarez VA, Cyras VP, Vazquez A (2008) Extraction of cellulose and preparation of nanocellulose from sisal fibers. Cellulose 15:149–159

Nagarajan S, Skillen NC, Irvine JTS, Lawton LA, Robertson PKJ (2017) Cellulose II as bioethanol feedstock and its advantages over native cellulose. Renew Sust Energ Rev 77:182–192

Nagarajan KJ, Balaji AN, Rajan STK, Ramanujam NR (2020) Preparation of bio-eco based cellulose nanomaterials from used disposal paper cups through citric acid hydrolysis. Carbohydr Polym 235:115997

Noorbakhsh-Soltani SM, Zerafat MM, Sabbhagi S (2018) A comparative study of gelatin and starch-based nanocomposite films modified by nano-cellulose and chitosan for food packaging applications. Carbohydr Polym 189:48–55

Normand ML, Moriana R, Ek M (2014) Isolation and characterization of cellulose nanocrystals from sprucebark in a biorefinery perspective. Carbohydr Polym 111:979–987

Noshirvani N, Hong W, Ghanbarzadeh B, Fasihi H, Montazami R (2018) Study of cellulose nanocrystal doped starch-polyvinyl alcohol bionanocomposite films. Int J Biol Macromol 107:2065–2074

Pei Y, Yang J, Liu P, Xu M, Zhang X, Zhang L (2013) Fabrication, properties, and bio-applications of cellulose/collagen hydrolysate composite films. Carbohydr Polym 92:1752–1760

Pereira PHF, Waldron KW, Wilson DR, Cunha AP, Brito ES, Rodrigues THS, Rosa MF, Azeredo HMC (2017) Wheat straw

hemicelluloses added with cellulose nanocrystals and citric acid: Effect on film physical properties. Carbohydr Polym 164:317–324

Perumal AB, Nambiar RB, Sellamuthu PS, Sadiku ER, Li X, He Y (2022) Extraction of cellulose nanocrystals from areca waste and its application in eco-friendly biocomposite film. Chemosphere 287:132084

Potenza M, Bergamonti L, Lottici PP, Righi L, Lazzarini L, Graiff C (2022) Green extraction of cellulose nanocrystals of polymorph II from *Cynara scolymus L.*: challenge for a "zero waste" economy. Crystals 12:672

Qin Z, Ji L, Yin Q, Zhu L, Lin Q, Qin J (2014) Synthesis and characterization of bacterial cellulose sulfates using a SO$_3$/pyridine complex in DMAc/LiCl. Carbohydr Polym 101:947–953

SaifulAzry SOA, Chuah TG, Paridah MT, Aung MM, Ridzuan MA, Lee CH, Sariah S, Lee SH, Juliana AH (2021) Influence of cellulose II polymorph nanowhiskers on bio-based nanocomposite film from Jatropha oil polyurethane. Mater Res Express 8:015003

Santos TM, Filho MM, Caceres CA, Rosa MF, Morais JPF, Pinto AMB, Azeredo HMZ (2014) Fish gelatin films as affected by cellulose whiskers and sonication. Food Hydrocoll 41:113–118

Sasikala M, Umapathy MJ (2018) Preparation and characterization of pineapple leaf cellulose nanocrystal reinforced gelatin bio-nanocomposite with antibacterial banana leaf extract for application in food packaging. RSC New J Chem 42:19979

Sathish M, Madhan B, Rao JR (2019) Leather solid waste: An ecobenign raw material for leather chemical preparation – A circular economy example. Waste Manag 87:357–367

Segal LGJMA, Creely JJ, Martin AE Jr, Conrad CM (1959) An empirical method for estimating the degree of crystallinity of native cellulose using the X-ray diffractometer. Text Res J 29:786–794

Uranga J, Leceta I, Extabide A, Guerrero P, de la Caba K (2016) Crosslinking of fish gelatins to develop sustainable films with enhanced properties. Eur Polym J 78:82–90

Wang HY, Li DG, Yano H, Abe K (2014) Preparation of tough cellulose II nanofibers with high thermal stability from wood. Cellulose 21:1505–1515

Wang S, Lu Y, Ouyang X-K, Ling J (2020) Fabrication of soy protein isolate/ cellulose nanocrystal composite nanoparticles for curcumin delivery. Int J Biol Macromol 165:1468–1474

Wu C-N, Saito T, Yang Q, Fukuzumi H, Isogai A (2014) Increase in water contact angle of composite film surfaces caused by the assembly of hydrophilic nanocellulose fibrils and nanoclay platelets. ACS Appl Mater Interfaces 6:12707–12712

Xiao Y, Liu Y, Kang S, Xu H (2021) Insight into in the formation mechanism of soy protein isolate films improved by cellulose nanocrystals. Food Chem 359:129971

Xing L, Hu C, Zhang W, Guan L, Gu J (2020) Biodegradable cellulose I (II) nanofibrils/poly(vinyl alcohol) composite films with high mechanical properties, improved thermal stability and excellent transparency. Int J Biol Macromol 164:1766–1775

Xu J, Salmi J, Kloser E, Perrin F, Grosse S, Denault J, Lau PCK (2013) Feasibility of nanocrystalline cellulose production by endoglucanase treatment of natural bast fibers. Ind Crop Prod 51:381–384

Xu X, Ouyang X-K, Yang L-Y (2021) Adsorption of (II) from aqueous solutions using crosslinked carboxylated chitosan/carboxylated nanocellulose hydrogel beads. J Mol Liq 322:114523

Yang W, He X, Luzi F, Dong W, Zheng T, Kenny JM, Puglia D, Ma P (2020) Thermomechanical, antioxidant, and moisture behavior of PVA films in presence of citric acid esterified cellulose nanocrystals. Int J Biol Macromol 161:617–626

Yu H, Qin Z, Liang B, Liu N, Zhou Z, Chen L (2013) Facile extraction of thermally stable cellulose nanocrystals with a high yield of 93% through hydrochloric acid hydrolysis under hydrothermal conditions. RSC J Mater Chemi A 1:3938–3944

Yu H-Y, Zhang D-Z, Lu F-F, Yao J (2016) New approach for single step extraction of carboxylated cellulose nanocrystals for their use as adsorbents and flocculants. ACS Sustain Chem Eng 4:2632–2643

Zhang J, Elder TJ, Pu Y, Ragauskas AJ (2007) Facile synthesis of spherical cellulose nanoparticles. Carbohydr Polym 69:607–611

Zhao Y, Zhang Y, Lindstrom ME, Li J (2015) Tunicate cellulose nanocrystals: Preparation, neat films and nanocomposite films with glucomannans. Carbohydr Polym 117:286–296

Zhao H, Ouyang X-K, Yang L-Y (2021) Adsorption of lead ions from aqueous solutions by porous cellulose nanofiber-sodium alginate hydrogel beads. J Mol Liq 324:115122